

Isothermal compression behavior of (Mg,Fe)O using neon as a pressure medium

Kirill K. Zhuravlev · J. M. Jackson · A. S. Wolf ·
J. K. Wicks · J. Yan · S. M. Clark

Received: 2 September 2009 / Accepted: 27 November 2009
© Springer-Verlag 2009

Abstract We present isothermal volume compression behavior of two polycrystalline (Mg,Fe)O samples with FeO = 39 and 78 mol% up to ~90 GPa at 300 K using synchrotron X-ray diffraction and neon as a pressure-transmitting medium. For the iron-rich (Mg_{0.22}Fe_{0.78})O sample, a structural transition from the B1 structure to a rhombohedral structure was observed at 41.6 GPa, with no further indication of changes in structural or compression behavior changes up to 93 GPa. In contrast, a change in the compression behavior of (Mg_{0.61}Fe_{0.39})O was observed during compression at $P \geq 71$ GPa and is indicative of a spin crossover occurring in the Fe²⁺ component of (Mg_{0.61}Fe_{0.39})O. The low-spin state exhibited a volume collapse of ~3.5%, which is a larger value than what was observed for a similar composition in a laser-heated NaCl medium. Upon decompression, the volume of the high-spin state was recovered at approximately 65 GPa. We therefore bracket the spin crossover at $65 \leq P$ (GPa) ≤ 77 at 300 K (Mg_{0.61}Fe_{0.39})O. We observed no deviation from the B1 structure in (Mg_{0.61}Fe_{0.39})O throughout the pressure range investigated.

Keywords (Mg,Fe)O · Lower mantle · Spin crossover · Phase transition

Introduction

(Mg,Fe)O ferropericlase is considered one of the main constituents of Earth's lower mantle, coexisting with perovskite-structured CaSiO₃ and (Mg,Fe)(Si,Al)O₃, and therefore plays an important role in the geophysics, geodynamics, and geochemistry of Earth's deep interior. In particular, the elastic properties of (Mg,Fe)O play a major role in the interpretation of seismological observations (Marquardt et al. 2009) and construction of geodynamic simulations (Bower et al. 2009). Investigations thus far indicate that (Mg,Fe)O forms a complete solid solution under ambient conditions. However, the exact chemical composition of (Mg,Fe)O throughout the lower mantle is dictated by bulk Earth starting composition (McDonough and Sun 1995) and phase equilibria (Irifune 1994; Murakami et al. 2005; Auzende et al. 2008; Sinmyo et al. 2008). Therefore, several studies have been performed to determine the pressure-dependent structural stability on samples with varying iron concentrations at ambient temperature (Mao et al. 1996; Shu et al. 1998; Mao et al. 2002; Jacobsen et al. 2005; Fei et al. 2007) and at high-temperatures (Jeanloz and Ahrens 1980; Knittle and Jeanloz 1986; Lin et al. 2003; Kondo et al. 2004).

(Mg_{1-x}Fe_x)O with $x < \sim 0.40$ has been the subject of several investigations because these compositions were determined to be in equilibrium with aluminum-bearing and aluminum-free pyrolite-like phase assemblages under shallow lower mantle conditions (e.g., Irifune 1994). After the detection of a spin crossover in the iron component of (Mg_{0.8}Fe_{0.2})O using X-ray emission spectroscopy (Badro

K. K. Zhuravlev · J. M. Jackson · A. S. Wolf · J. K. Wicks
Seismological Laboratory, Division of Geological and Planetary
Sciences, California Institute of Technology,
Pasadena, CA 91125, USA

J. Yan · S. M. Clark
Advanced Light Source, Lawrence Berkeley National
Laboratory, Berkeley, CA 94720, USA

Present Address:

K. K. Zhuravlev (✉)
Department of Chemistry, University of Western Ontario,
London, ON N6A 5B7, Canada
e-mail: kirillzhuravlev@gmail.com

et al. 2003), several studies have shown that a correlation exists between the spin crossover in iron-poor (Mg,Fe)O and a change in physical properties such as density (Lin et al. 2005; Speziale et al. 2007) and sound velocities (Lin et al. 2006; Crowhurst et al. 2008; Marquardt et al. 2009). X-ray diffraction studies on (Mg_{1-x}Fe_x)O with $x = 0.20$, 0.39 and 0.58 using laser-annealing and NaCl as a pressure medium reported spin crossover pressures of ~ 40 , 60, and 80 GPa, respectively, based on observed changes in compression behavior (Fei et al. 2007). Using neon as a pressure-transmitting medium, Lin et al. (2005) observed changes in the compression behavior of (Mg_{0.83}Fe_{0.17})O at $P \sim 55$ GPa. A positive correlation in crossover pressure as a function of increasing iron concentration in (Mg,Fe)O is in qualitative agreement with crystal-field and mean-field calculations that include cooperative interactions (Sturhahn et al. 2005), density functional theoretical calculations (Persson et al. 2006; Tsuchiya et al. 2006), and ab initio calculations including iron-clustering (Kantor et al. 2009).

Fewer investigations have been performed on Fe-rich (Mg,Fe)O under lower mantle conditions. Studies conducted in a helium pressure medium indicate that FeO wüstite undergoes a displacive phase transition from the NaCl-*B1* (space group $Fm\bar{3}m$) to a rhombohedral (space group $R\bar{3}m$) structure at 18 GPa for Fe_{0.94}O (Shu et al. 1998) and 23 GPa for Fe_{0.93}O (Jacobsen et al. 2005), whereas MgO-periclase remains in the *B1* structure to at least 227 GPa (Duffy et al. 1995). It has been suggested from various studies that decreasing the Fe content in (Mg_{1-x}Fe_x)O for $x > 0.50$ causes an increase in the pressure at which the phase transition from the cubic to rhombohedral structure occurs (Mao et al. 1996, 2002; Shu et al. 1998; Lin et al. 2003; Fei et al. 2007). However, there are discrepancies in reported trends in the transition pressure as a function of iron concentration, which are likely due to different stress conditions achieved in different investigations.

In this study, we conducted high-pressure powder X-ray diffraction experiments in pressure steps of ~ 2 GPa at 300 K on (Mg_{0.22}Fe_{0.78})O to 93 GPa and (Mg_{0.61}Fe_{0.39})O to 90 GPa using neon as a pressure medium. Such measurements extend the P - V space covered for (Mg_{0.22}Fe_{0.78})O and permit one to evaluate the effect of different pressure media on the pressure at which the rhombohedral structural transition occurs in iron-rich (Mg,Fe)O and the onset of the change in compression behavior due to the spin crossover in iron-poor (Mg,Fe)O.

Experiment

We used a portion of a single-crystal of (Mg_{0.22}Fe_{0.78})O for this study that was synthesized according to the procedure

described by Mackwell et al. (2005) by interdiffusion of iron oxide powders into a single-crystal of MgO. Complete characterization at ambient conditions was reported in Jacobsen et al. (2002). Independent electron microprobe analysis was carried out on the JEOL JXA-8200 5-spectrometer at Caltech to ensure the sample quality and uniformity. The average sample composition is (Mg_{0.206(1)}Fe_{0.780(1)}Ca_{0.0011(1)}Al_{0.0089(3)})O, where the digits in parentheses indicate the standard deviation of the last significant digit based on 10 different spots approximately 10 μm apart on the bulk single-crystal. The iron-poor (Mg,Fe)O polycrystalline sample was synthesized from powders of Fe₂O₃ and fired MgO in a CO/CO₂ gas-mixing furnace at 1,473 K and $\log f\text{O}_2 = -10$ for a total of ~ 120 h. The synthesis was carried out in three runs, each lasting ~ 40 h. For each run, the oxide powders were re-ground, mixed together and pressed into a pellet. Samples were quenched into a cold reservoir of the same gas mixture. Microprobe analysis yielded the following composition: (Mg_{0.61(2)}Fe_{0.39(3)})O.

Two symmetric-type piston cylinder diamond-anvil cells were used in our experiments. We used beveled anvils having a flat culet diameter of 250 μm , and each cell was prepared with a different sample composition. A 100 μm diameter hole was drilled in two different Re gaskets pre-indented to a thickness of 30 μm . Ruby spheres were used as pressure markers and were loaded into the sample chamber of each cell together with the polycrystalline sample. Neon was used as a pressure-transmitting medium. Gas-loading of neon into the sample chambers was done at GSECARS at the Advanced Photon Source of Argonne National Laboratory at 25,000 PSI (Rivers et al. 2008). The final hole diameter decreased to ~ 50 μm after sealing the Ne into the sample chamber. The pressure was determined using the R1 ruby fluorescence line shift reported by Jacobsen et al. (2008), where the authors re-calibrated the R1 line shift to the P - V behavior of MgO using helium as a pressure medium:

$$P(\text{GPa}) = A/B \left(\left[\frac{\lambda}{\lambda_0} \right]^B - 1 \right) \quad (1)$$

where $A = 1904$, $B = 10.32$, and λ_0 is the zero-pressure wavelength ($\lambda_0 = 694.24$ nm in this study). We chose this pressure scale based on the assumption that neon as a pressure medium exhibits stress conditions closer to that of helium, in comparison to argon (Mao et al. 1986), for pressures greater than ~ 50 GPa. Typical ruby spectra are shown in Fig. 1. The R1 and R2 fluorescence lines remain well-resolved even at the highest pressure, which indicates adequate stress conditions throughout the experimental run. We report the uncertainty in pressure as the average pressure and standard deviation determined immediately before

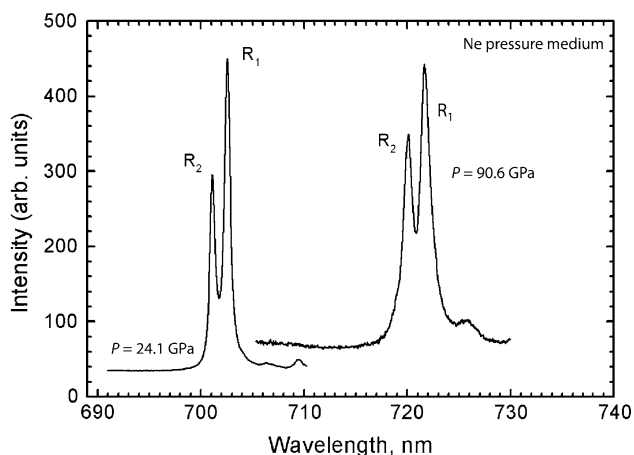
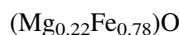


Fig. 1 Fluorescence spectra of the ruby sphere in the sample chamber at 24.1 and 90.6 GPa. Note that the R1 and R2 peaks are well-resolved at 90.6 GPa, although some broadening is observed

and after diffraction data were collected. Therefore, the uncertainty in pressure given in Tables 1, 2, 3, and 5 reflects the pressure drift over the time required to collect an XRD pattern not the uncertainty in pressure, which is likely to be closer to 3%. Experiments were performed at beamline 12.2.2 of the Advanced Light Source at Lawrence

Berkeley National Laboratory. The beam was collimated to $10 \times 10 \mu\text{m}$. We collected X-ray diffraction spectra using an incident energy of 30 keV ($\lambda = 0.4133 \text{ \AA}$) and a high-resolution MAR image plate to collect the diffracted photons. The diffraction images were integrated using Fit2D (Hammersley et al. 1996) and whole profile analysis was done using the GSAS + EXPGUI package (Larsen and Von Dreele 2000; Toby 2001). The errors in volume are determined from the GSAS fit, but are likely to be underestimated. All P - V data were fit to Birch–Murnaghan and Vinet equations of state (EOS) using the EOS-FIT (V5.2) least-squares package (Angel 2000).

Results and discussion



We compressed powdered $(\text{Mg}_{0.22}\text{Fe}_{0.78})\text{O}$ in the pressure range from 7.9 to 92.9 GPa, with pressure increments of approximately 1–2 GPa, at 300 K. Typical integrated X-ray diffraction spectra are shown in Fig. 2. With increasing pressure, we were able to reliably identify the 111 and 200 reflections, corresponding to the cubic $B1$

Table 1 Volume per atom (V_{atom}) for $(\text{Mg}_{0.22}\text{Fe}_{0.78})\text{O}$ as a function of pressure at 300 K

P_{ruby}^* (GPa)	$V_{\text{pfu}} (\text{\AA}^3)$	σ_P^* (GPa)	$\sigma_V (\text{\AA}^3)$	P_{ruby}^* (GPa)	$V_{\text{pfu}} (\text{\AA}^3)$	σ_P^* (GPa)	$\sigma_V (\text{\AA}^3)$
7.9	9.401	0.1	0.017	52.8	7.848	0.1	0.026
9.2	9.317	0.1	0.198	54.3	7.812	0.1	0.029
10.8	9.245	0.1	0.032	55.3	7.774	0.2	0.055
13.0	9.138	0.1	0.059	56.8	7.722	0.2	0.051
14.9	9.074	0.1	0.137	59.1	7.681	0.3	0.137
16.3	9.016	0.1	0.088	61.1	7.641	0.2	0.048
17.8	8.945	0.1	0.044	62.6	7.621	0.3	0.067
24.1	8.726	0.1	0.055	65.0	7.581	0.1	0.066
26.5	8.671	0.2	0.014	66.8	7.523	0.3	0.096
27.5	8.609	0.2	0.12	68.8	7.495	0.2	0.079
30.4	8.52	0.1	0.056	71.2	7.401	0.3	0.045
32.4	8.477	0.1	0.031	72.9	7.383	0.4	0.125
33.3	8.439	0.2	0.052	74.2	7.32	0.3	0.046
34.9	8.445	0.1	0.123	77.3	7.264	0.4	0.009
36.3	8.312	0.1	0.149	79.4	7.222	0.3	0.092
38.6	8.314	0.1	0.175	81.1	7.201	0.4	0.016
39.8	8.283	0.2	0.022	82.9	7.196	0.6	0.065
41.6	8.172	0.1	0.06	85.3	7.112	0.2	0.010
42.9	8.135	0.1	0.078	86.5	7.052	0.4	0.188
43.9	8.106	0.1	0.041	87.6	7.031	0.4	0.008
44.8	8.079	0.1	0.052	89.2	6.994	0.4	0.012
46.7	8.041	0.2	0.059	90.6	6.962	0.4	0.089
47.5	8.005	0.1	0.055	92.9	6.933	0.5	0.072
48.9	7.967	0.1	0.039				
51.3	7.877	0.2	0.055				

The average pressure (P_{ruby}^*) and standard deviation (σ_P^*) was determined immediately before and after diffraction data were collected. Therefore, the σ_P reflects the pressure drift over the time required to collect an XRD pattern not the uncertainty in pressure, which is likely to be closer to 3%

Table 2 Pressure–volume (P – V) data for $(\text{Mg}_{0.22}\text{Fe}_{0.78})\text{O}$ (B1)

P_{ruby}^* (GPa)	V (\AA^3)	σ_p^* (GPa)	σ_v (\AA^3)
7.9	75.205	0.1	0.136
9.2	74.539	0.1	1.587
10.8	73.961	0.1	0.259
13.0	73.103	0.1	0.470
14.9	72.595	0.1	1.099
16.3	72.132	0.1	0.700
17.8	71.561	0.1	0.353
24.1	69.807	0.1	0.437
26.5	69.371	0.2	0.113
27.5	68.876	0.2	0.960
30.4	68.157	0.1	0.450
32.4	67.817	0.1	0.245
33.3	67.514	0.2	0.415
34.9	67.558	0.1	0.983
36.3	66.494	0.1	1.193
38.6	66.509	0.1	1.396
39.8	66.268	0.2	0.177

* Symbols have the same meaning as in Table 1

($Fm\bar{3}m$) structure, up to $P = 41.6$ GPa. In Fig. 3, we plot the volume per atom of $(\text{Mg}_{0.22}\text{Fe}_{0.78})\text{O}$ as a function of pressure and note that there is no obvious change in the compression behavior over the pressure range investigated (Fig. 3), consistent with observations made earlier on similar compositions (Richet et al. 1989; Mao et al. 2002; Jacobsen et al. 2005; Fei et al. 2007).

At 41.6 GPa, the 111 peak of the B1 structure split into two distinct peaks. We interpret this indication of the phase transition in Fe-rich $(\text{Mg,Fe})\text{O}$ from the cubic ($Fm\bar{3}m$) to the rhombohedral $R\bar{3}m$ structure, where the cubic 111 peak splits into the rhombohedral 003 and 101 peaks (e.g., Mao et al. 2002). At 41.6 GPa, we also observed a splitting of the 200 peak. Normalized pressure (F) versus Eulerian finite strain (f) (Angel 2000) for the entire pressure range of our experiment on $(\text{Mg}_{0.22}\text{Fe}_{0.78})\text{O}$ is shown as an inset to Fig. 3. A distinct change in the trend of data is observed at a strain corresponding to $P = 41.6$ GPa. Our results on $(\text{Mg}_{0.22}\text{Fe}_{0.78})\text{O}$ indicate a structural phase transition from cubic to a rhombohedral structure occurred on compression at $39.8 < P$ (GPa) < 41.6 . For comparison, earlier works using no pressure medium on a suite of iron-rich $(\text{Mg,Fe})\text{O}$ compositions (FeO = 80, 90, and 95 mol%) and $\text{Fe}_{0.95}\text{O}$ reported no compositional effect on transition pressure of $P = 16$ GPa (Kondo et al. 2004), whereas experiments using helium as a pressure medium reported transition pressures of ~ 20 GPa for FeO $\geq 90\%$ (Mao et al. 1996, 2002; Shu et al. 1998; Jacobsen et al. 2005). An XRD investigation of $(\text{Mg}_{0.25}\text{Fe}_{0.75})\text{O}$ using NaCl as a pressure medium indicated a transition pressure of 60 GPa to the

Table 3 P – V data for $(\text{Mg}_{0.22}\text{Fe}_{0.78})\text{O}$ (rhombohedral structure)

P_{ruby}^* (GPa)	a (\AA)	b (\AA)	V (\AA^3)	σ_p^* (GPa)	σ_v (\AA^3)
41.6	2.8237	7.0687	49.034	0.1	0.361
42.9	2.8195	7.0648	48.810	0.1	0.465
43.9	2.8155	7.0612	48.638	0.1	0.243
44.8	2.8094	7.0581	48.475	0.1	0.310
46.7	2.8039	7.0543	48.244	0.2	0.352
47.5	2.7985	7.0483	48.030	0.1	0.332
48.9	2.8213	7.1487	47.804	0.1	0.235
51.3	2.7853	7.0348	47.264	0.2	0.329
52.8	2.7809	7.0306	47.086	0.1	0.154
54.3	2.7754	7.0265	46.873	0.1	0.173
55.3	2.7693	7.0231	46.644	0.2	0.339
56.8	2.763	7.008	46.333	0.2	0.306
59.1	2.8235	6.675	46.085	0.3	0.820
61.1	2.7515	6.9928	45.848	0.2	0.290
62.6	2.7485	6.9895	45.727	0.3	0.400
65.0	2.7425	6.9835	45.488	0.1	0.394
66.8	2.7335	6.9755	45.138	0.3	0.576
68.8	2.729	6.972	44.967	0.2	0.472
71.2	2.715	6.956	44.405	0.3	0.269
72.9	2.7123	6.9532	44.299	0.4	0.752
74.2	2.7023	6.9452	43.922	0.3	0.276
77.3	2.6945	6.9317	43.584	0.4	0.053
79.4	2.688	6.925	43.332	0.3	0.549
81.1	2.6853	6.9183	43.203	0.4	0.093
82.9	2.6856	6.912	43.173	0.6	0.389
85.3	2.6733	6.8943	42.669	0.2	0.057
86.5	2.663	6.8894	42.311	0.4	1.125
87.6	2.6612	6.8783	42.186	0.4	0.048
89.2	2.659	6.8534	41.964	0.4	0.074
90.6	2.6536	6.8494	41.769	0.4	0.532
92.9	2.649	6.8451	41.598	0.5	0.431

Errors on the lattice parameters are 3%

* Symbols have the same meaning as in Table 1

rhombohedral structure (Lin et al. 2003). Using similar experimental conditions as Lin et al. (2003), Fei et al. (2007) reported that $(\text{Mg}_{0.42}\text{Fe}_{0.58})\text{O}$ transforms into a rhombohedral structure at about 44 GPa. Such a discrepancy in trends is due to the sensitivity of the transition pressure to nonhydrostatic conditions. Our experiment was done using neon as a pressure medium, which provided low deviatoric stress conditions throughout the pressure range investigated (Fig. 1). Our results for $(\text{Mg}_{0.22}\text{Fe}_{0.78})\text{O}$ are in qualitative agreement with results obtained using other pressure media (Fig. 4), however, the scatter in the results obtained by using NaCl and laser-annealing produce different trends for less iron-concentrated samples (Lin et al. 2003; Fei et al. 2007).

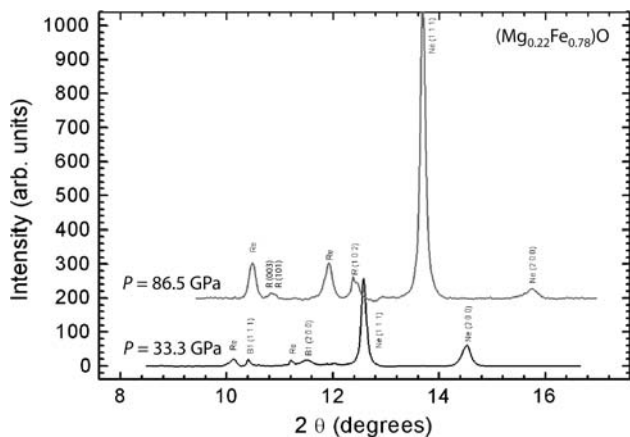


Fig. 2 Integrated X-ray spectra of $(\text{Mg}_{0.22}\text{Fe}_{0.78})\text{O}$ at 33.3 GPa and 86.5 at 300 K. At 86.5 GPa, both the 111 and 200 peaks of the B1 structure of are split, indicating a phase transition has occurred

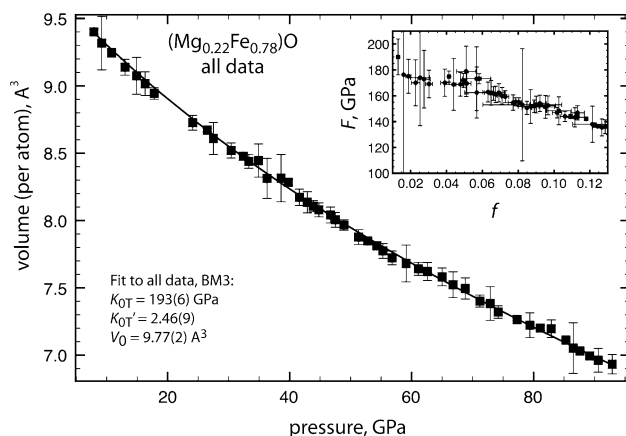


Fig. 3 Volume per atom for entire pressure range investigated (Table 1). *Solid line* is the fit to the third-order Birch–Murnaghan EOS (Table 4). *Inset* normalized pressure (F) versus Eulerian finite strain (f) for $(\text{Mg}_{0.22}\text{Fe}_{0.78})\text{O}$ with $V_0 = 9.77 \pm 0.02 \text{ \AA}^3$. A distinct change of slope is seen at a strain corresponding to $P = 41.6 \text{ GPa}$

We now separate the P – V trends according to structural state and analyze the equations of state. The P – V data for the cubic phase of $(\text{Mg}_{0.22}\text{Fe}_{0.78})\text{O}$ are shown in Table 2 and Fig. 5. The P – V data for the cubic phase of $(\text{Mg}_{0.22}\text{Fe}_{0.78})\text{O}$ is well fit to a second-order Birch–Murnaghan equation of state, yielding the following thermodynamic parameters $V_0 = 78.49 \pm 0.210 \text{ \AA}^3$, $K_{0T} = 166 \pm 5 \text{ GPa}$ (K'_{0T} fixed to 4). A fit to a third-order Birch–Murnaghan equation of state produced the following parameters: $V_0 = 78.74 \pm 0.57 \text{ \AA}^3$, $K_{0T} = 152 \pm 28 \text{ GPa}$, and $K'_{0T} = 4.8 \pm 1.7$. A fit constrained by the Vinet EOS yielded values within the respective uncertainties of those given by the Birch–Murnaghan EOS. The summary of all fitting results is presented in Table 4. Our elastic parameters are in good agreement with ultrasonic measurements on single-crystals of similar compositions at ambient conditions, isothermal single-

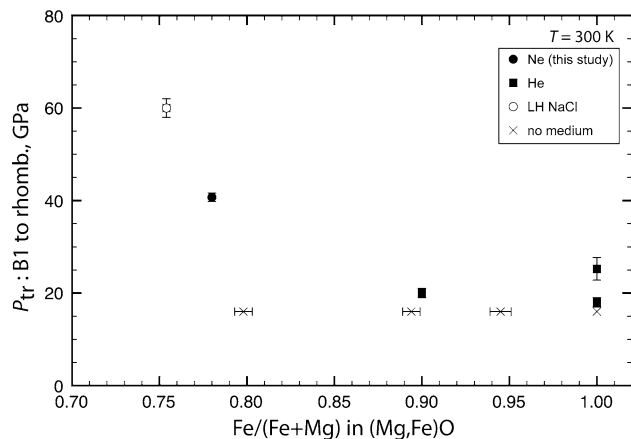


Fig. 4 Transition pressure of the cubic B1 to rhombohedral structure in iron-rich $(\text{Mg,Fe})\text{O}$, as reported by different investigations using different pressure media. *Solid symbols* are transition pressures reported from experiments using helium ($\text{Fe}_{0.95}\text{O}$, Jacobsen et al. 2005, $P_{\text{tr}} = 23 \text{ GPa}$; $\text{Fe}_{0.94}\text{O}$, Shu et al. 1998, $P_{\text{tr}} = 18 \text{ GPa}$; $\text{FeO} = 90\%$, Mao et al. 2002) and neon ($\text{FeO} = 78\%$, this study). The *open circle* is from a study using laser-annealing and NaCl as a pressure medium ($\text{FeO} = 75 \text{ mol\%}$, Lin et al. 2003). *Crosses* indicate a study using no pressure medium ($\text{FeO} = 94.5, 89.4, \text{ and } 79.8 \text{ mol\%}$ and $\text{Fe}_{0.95}\text{O}$, Kondo et al. 2004). We plot the uncertainties in the composition and transition pressure from those given in the respective references

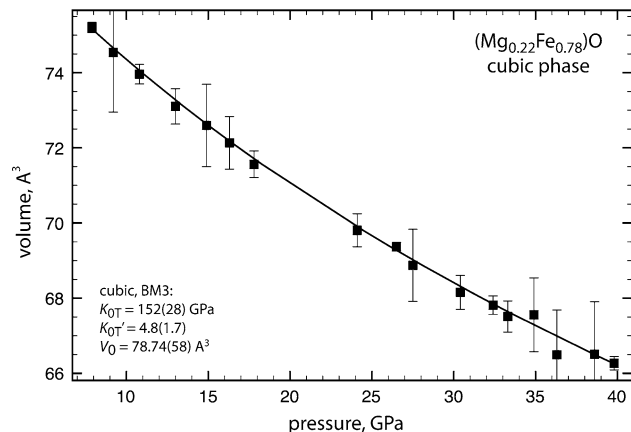


Fig. 5 P – V data for the cubic phase of $(\text{Mg}_{0.22}\text{Fe}_{0.78})\text{O}$. *Solid squares* indicate compression data from this study using neon as a pressure medium (Table 2). The *black solid line* is a Birch–Murnaghan 3rd EOS fit to our data (Table 4)

crystal compression results on $(\text{Mg}_{0.25}\text{Fe}_{0.72}\square_{0.04})\text{O}$ to $P = 7.2 \text{ GPa}$ (Jacobsen et al. 2002), and X-ray powder diffraction studies on $(\text{Mg}_{0.1}\text{Fe}_{0.9})\text{O}$ (Mao et al. 2002).

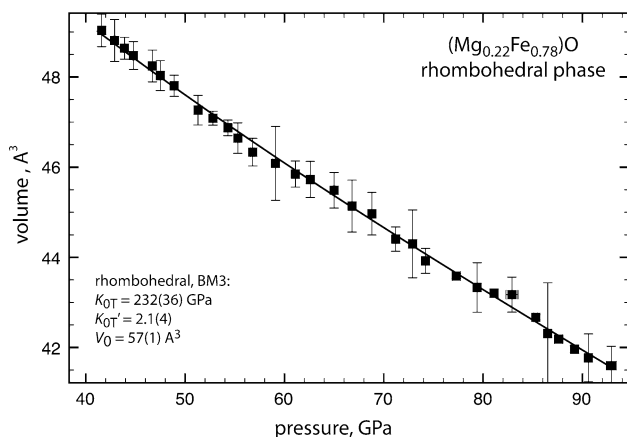
Assuming the rhombohedral ($R\bar{3}m$) space group, we analyzed our spectra in the pressure range from 41.6 GPa, the onset of the 111 and 200 peak splitting, to the highest pressure achieved, 92.9 GPa (Table 3). We obtained the following parameters for the third-order Birch–Murnaghan EOS: $V_0 = 57 \pm 1 \text{ \AA}^3$, $K_{0T} = 232 \pm 36 \text{ GPa}$, $K'_{0T} = 2.1 \pm 0.4$ (Figs. 6, 7). If one assumes a Vinet EOS, one

Table 4 Equation of state parameters for $(\text{Mg}_{0.22}\text{Fe}_{0.78})\text{O}$ for different types of EOS

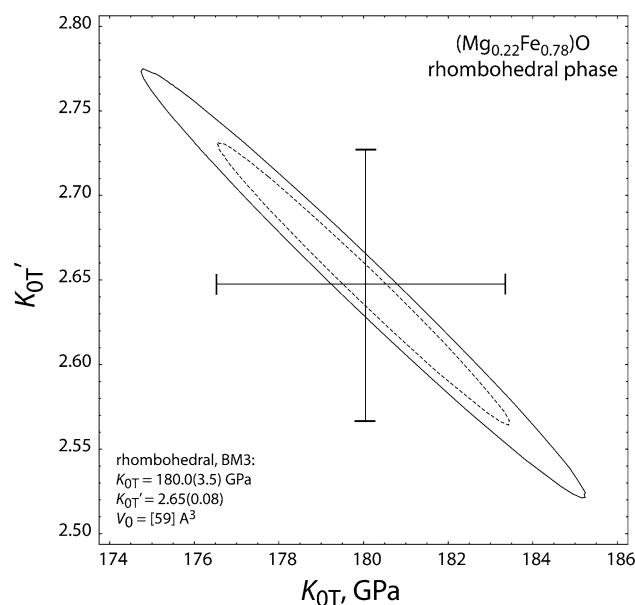
	V_0 (\AA^3)	K_{0T} (GPa)	K'_{0T}	χ_w^2
Cubic phase ($B1$, $Fm\bar{3}m$)				
B-M 2nd order	78.49(21)	166(5)	[4]	0.13
Vinet	78.46(21)	168(5)	[4]	0.14
B-M 3rd order	78.74(57)	152(28)	4.8(1.7)	0.12
Vinet	78.77(58)	150(29)	5.1(1.6)	0.12
Rhombohedral phase ($R\bar{3}m$)				
B-M 3rd order*	[59]	180.0(3.5)	2.65(0.08)	0.28
B-M 3rd order	57(1)	232(36)	2.1(4)	0.30
Vinet	56(1)	290(64)	0.3(1)	0.30
Fit to the entire pressure range using volume per atom (V_{atom})				
	$V_{0\text{-atom}}$ (\AA^3)	K_{0T} (GPa)	K'_{0T}	χ_w^2
B-M 3rd order	9.77(2)	193(6)	2.46(9)	0.40
Vinet	9.74(2)	206(7)	1.7(2)	0.40

Weighted fitting was performed based on our reported uncertainties in pressure and volume. Numbers in parentheses indicate the esd's for the last digit for the last reported significant digit(s). Numbers in square brackets are fixed in the fitting procedure

* Constrained to the theoretical volume of 3/4 the V_0 for the B1 structure (Fig. 7)


Fig. 6 P - V data for the rhombohedral phase of $(\text{Mg}_{0.22}\text{Fe}_{0.78})\text{O}$ obtained using neon as a pressure medium (Table 3). *Solid line* is the fit to a third-order Birch–Murnaghan EOS (Table 4)

obtains significantly different values for the elastic parameters and in general, the values of K'_{0T} are unusually low (Table 4). Although our pressure–volume sampling space is very dense for the rhombohedral structure, significantly large errors arise upon fitting all three parameters due to the large trade-off between K_{0T} and K'_{0T} . We therefore constrained the V_0 of the rhombohedral phase to be the theoretical value of 3/4 the V_0 for the B1 phase, $V_0 = 59 \text{ \AA}^3$ and obtain the following $K_{0T} = 180 \pm 3.5$ GPa, $K'_{0T} = 2.65 \pm 0.08$ (Table 4). The confidence ellipses are shown for this fit in Fig. 7. We note that Richet


Fig. 7 Evaluation of the trade-off between K_{0T} and K'_{0T} for the third-order Birch–Murnaghan EOS fit to the P - V data for $(\text{Mg}_{0.22}\text{Fe}_{0.78})\text{O}$ in the rhombohedral phase when V_0 is fixed to 59 \AA^3 , the theoretical volume calculated from 3/4 the V_0 of the B1 phase (Table 4). *Error bars* illustrate ± 1 esd. The *dashed* and the *solid* confidence ellipses are centered at the 68.3% level and two degrees of freedom (independently determined K_{0T} and K'_{0T})

et al. (1989) reported unusually low values of K'_{0T} for iron-rich $(\text{Mg},\text{Fe})\text{O}$ from a fit to their entire data set up to ~ 50 GPa.

In the pressure range of 10 to ~ 50 GPa, iron-rich $(\text{Mg},\text{Fe})\text{O}$ undergoes a magnetic transition from the paramagnetic to a magnetically ordered state at 300 K, according to conventional Mössbauer measurements (Kantor et al. 2004; Speziale et al. 2005). The changes in magnetism are not necessarily occurring at the same pressure as the onset of the rhombohedral distortion (Kantor et al. 2004). Ultrasonic interferometry measurements up to ~ 9 GPa on a single-crystal of $(\text{Mg}_{0.22}\text{Fe}_{0.78})\text{O}$ showed a softening of the shear elastic constant C_{44} throughout the investigated pressure range (Jacobsen et al. 2004). Nuclear resonant inelastic X-ray scattering measurements on wüstite showed that a softening of the Fe-weighted partial phonon density of states occurring at $P = 10$ GPa persisting up to their highest pressure achieved, 49 GPa (Struzhkin et al. 2001). Therefore, we suggest that the equations of state for the distinct structural states determined from static X-ray diffraction measurements may not be accurate in the vicinity of the magnetic transition.

We did not observe any obvious indication of a change in the P - V trajectory of $(\text{Mg}_{0.22}\text{Fe}_{0.78})\text{O}$ in our study. The onset of the crossover from the paramagnetic or magnetically ordered state (high-spin) to the diamagnetic state

(low-spin) in (Mg,Fe)O depends on the Fe^{2+} concentration and temperature (Sturhahn et al. 2005; Tsuchiya et al. 2006), as well as thermal history of the sample (Kantor et al. 2009). Computational studies show that increasing the iron concentration leads to an increase in the crossover pressure (Sturhahn et al. 2005; Persson et al. 2006). For iron-rich (Mg,Fe)O, the series of magnetic and structural transitions at 300 K are different than those of iron-poor (Mg,Fe)O. The crossover from a magnetically ordered state (high-spin) to a diamagnetic (low-spin) state was investigated using conventional Mössbauer spectroscopy, but without a pressure medium, and the crossover pressure was reported to occur at about 80 GPa for $(\text{Mg}_{0.2}\text{Fe}_{0.8})\text{O}$ and 90 GPa for $\text{Fe}_{0.97}\text{O}$ (Speziale et al. 2005). It is clear that XRD is not a direct means to detect changes in magnetic states. However, if the crossover from a magnetically ordered state (high-spin) to a diamagnetic state (low-spin) exhibits a volume change, we conclude that either this particular crossover did not occur in $(\text{Mg}_{0.22}\text{Fe}_{0.78})\text{O}$ in the pressure range investigated or that the crossover is not associated with a change in compression trajectory.

$(\text{Mg}_{0.61}\text{Fe}_{0.39})\text{O}$

X-ray powder diffraction spectra of $(\text{Mg}_{0.61}\text{Fe}_{0.39})\text{O}$ were measured up to 89.7 GPa and with decreasing pressure at 300 K (Table 5). We did not observe any obvious peak splitting in the $(\text{Mg}_{0.61}\text{Fe}_{0.39})\text{O}$ spectra, indicating this composition remains in the cubic phase throughout the pressure range investigated (Fig. 8) (Lin et al. 2003; Fei et al. 2007). The volume compression of powdered $(\text{Mg}_{0.61}\text{Fe}_{0.39})\text{O}$ clearly shows that there is a change in compression behavior starting at $P \geq 71$ GPa, indicative of the onset of a spin crossover (Fig. 9) (Lin et al. 2005; Sturhahn et al. 2005; Fei et al. 2007).

The data for the high-spin state ($15.5 \leq P$ (GPa) ≤ 70.9) was fit to a second- and third-order Birch–Murnaghan EOS with the following results: $V_0 = 77.4 \pm 0.2 \text{ \AA}^3$ and $K_{0T} = 161 \pm 3$ GPa with $K'_{0T} = 4$ (fixed) (Fig. 9). These values are in good agreement with the values reported from room-pressure ultrasonic measurements on a similar composition (Jacobsen et al. 2002) and from diffraction measurements in a laser-annealed NaCl pressure medium (Fei et al. 2007). Similar results were obtained for the third-order Birch–Murnaghan and Vinet EOS (Table 6). We plot normalized stress (F) versus Eulerian finite strain (f), where we assume V_0 is the same for each spin state (inset Fig. 9). With increasing pressure, the F – f trajectory becomes negative for only a finite pressure range in the vicinity of the pressure range where other methods have confirmed the occurrence of a spin crossover. At $P = 72.2$ GPa, the onset volume collapse is observed and at $P \geq 76.6$ GPa, $(\text{Mg}_{0.61}\text{Fe}_{0.39})\text{O}$ is likely to

be in the low-spin state based on the compression trajectory. The number of data points and total compression range were not sufficient to satisfactorily constrain the EOS through the spin crossover, though. The region of P – V space where the compression trajectory changes in response to the crossover is associated with a negative derivative of bulk modulus with increasing pressure, because $K_T = -V(\partial P/\partial V)_T$. A softening of the compressional wave velocities of iron-poor (Mg,Fe)O has been reported (Crowhurst et al. 2008), and studies to determine the shear velocities show that there is little to no increase in select shear modes as pressure is increased in the vicinity of the spin crossover (Lin et al. 2006; Marquardt et al. 2009). This is contrary to the behavior of MgO, where the compressional and shear waves increase steadily with increasing pressure (Zha et al. 2000; Murakami et al. 2005).

Upon decompression, the transition back to the high-spin state (based on P – V trajectory) was completed at about 65 GPa, resulting in a hysteresis of ~ 10 GPa (Fig. 9). Although neon is soft relative to alternative media like NaCl or argon, neon is certainly not hydrostatic at these pressures. The hysteresis observed in this study is likely due to the build up of strain in the crystallites. The resulting decompression hysteresis can be viewed as the low-spin state persisting in a metastable state until the Jahn–Teller distortion of the high-spin state is favored. The hysteresis therefore represents bounds on the crossover pressure to $65 \leq P$ (GPa) ≤ 77 for $(\text{Mg}_{0.61}\text{Fe}_{0.39})\text{O}$ at 300 K.

Conclusions

We conducted high-pressure powder X-ray diffraction experiments in pressure steps of ~ 2 GPa at 300 K on $(\text{Mg}_{0.22}\text{Fe}_{0.78})\text{O}$ to 93 GPa and $(\text{Mg}_{0.61}\text{Fe}_{0.39})\text{O}$ to 90 GPa using neon as a pressure medium. Such measurements extend the P – V space covered for $(\text{Mg}_{0.22}\text{Fe}_{0.78})\text{O}$ and permit one to evaluate the effect of different pressure media on the pressure at which the rhombohedral structural transition occurs in iron-rich (Mg,Fe)O. Incorporating measurements on different iron contents using helium as a pressure medium, we find a steep dependence on the structural transition pressure from the cubic to rhombohedral phase as magnesium is added to the end-member wüstite in the (Mg,Fe)O solid solution at 300 K (Fig. 4).

We determined that $(\text{Mg}_{0.61}\text{Fe}_{0.39})\text{O}$ remains in the cubic $B1$ phase throughout the range of our experimental pressures, consistent with previous studies (e.g., Lin et al. 2003; 2005; Fei et al. 2007). Therefore, a change in the P – V trajectory at $P \sim 72$ GPa was observed without evidence of a structural transition in our study. The onset of the change in compression behavior found in our study

Table 5 P - V data for $(\text{Mg}_{0.61}\text{Fe}_{0.39})\text{O}$ (B1) on compression and decompression

P_{ruby}^* (GPa)	V (\AA^3)	σ_P^* (GPa)	σ_V (\AA^3)	P_{ruby}^* (GPa)	V (\AA^3)	σ_P^* (GPa)	σ_V (\AA^3)
Compression							
15.5	70.722	0.3	0.041	54.7	62.109	0.25	0.076
18.4	70.435	0.5	0.086	55.4	62.113	0.25	0.084
20.3	69.543	0.5	0.049	56.1	62.000	0.25	0.083
22.0	69.482	0.5	0.080	56.8	61.991	0.10	0.081
24.2	68.795	0.5	0.086	57.9	61.658	0.30	0.069
25.4	68.393	0.4	0.046	58.8	61.564	0.10	0.067
26.8	68.257	0.5	0.058	59.4	61.457	0.20	0.091
28.0	67.892	0.5	0.060	60.1	60.965	0.10	0.082
29.6	67.519	0.3	0.055	60.9	61.107	0.10	0.065
30.7	67.116	0.3	0.072	61.4	60.963	0.15	0.081
32.2	67.097	0.45	0.098	62.2	60.763	0.10	0.085
33.4	66.184	0.3	0.077	63.7	60.504	0.10	0.096
34.5	66.057	0.3	0.067	65.2	60.241	0.15	0.095
35.7	65.856	0.3	0.092	68.5	59.630	0.30	0.106
36.7	65.431	0.5	0.070	70.9	59.461	0.10	0.112
38.0	65.446	0.2	0.061	72.2	58.515	0.15	0.183
39.1	64.824	0.3	0.071	74.0	57.606	0.25	0.152
40.7	64.558	0.25	0.090	76.6	56.987	0.10	0.168
41.7	64.255	0.4	0.098	78.3	56.579	0.05	0.181
43.2	64.438	0.3	0.116	79.8	56.261	0.05	0.173
44.9	63.990	0.35	0.076	80.8	56.235	0.10	0.169
46.3	63.890	0.45	0.088	82.1	56.208	0.05	0.103
48.1	63.473	0.5	0.083	84.0	55.870	0.15	0.085
49.9	63.149	0.2	0.076	86.2	55.634	0.05	0.090
50.8	62.831	0.25	0.072	88.5	55.245	0.05	0.094
51.9	62.722	0.15	0.082	89.7	55.015	0.05	0.110
52.8	62.656	0.25	0.089				
53.6	62.401	0.25	0.081				
Decompression							
57.4	62.30636	0.5	0.104				
58.3	61.92993	0.5	0.121				
61.76	61.28415	0.05	0.114				
63.4	60.84685	0.4	0.135				
65.76	59.86825	0.05	0.345				
67.8	58.25765	0.2	0.581				
69.4	57.28479	0.3	0.163				
70.8	57.49011	0.2	0.106				
73.25	57.03106	0.05	0.091				
75.4	56.72934	0.2	0.121				
77.40	56.52584	0.05	0.097				
78.94	56.26114	0.05	0.093				
80.03	55.97092	0.05	0.148				
82.0	55.74735	0.2	0.127				
84.21	55.54184	0.05	0.131				
86.20	55.31941	0.05	0.193				
87.2	55.15406	0.1	0.222				

* Symbols have the same meaning as in Table 1

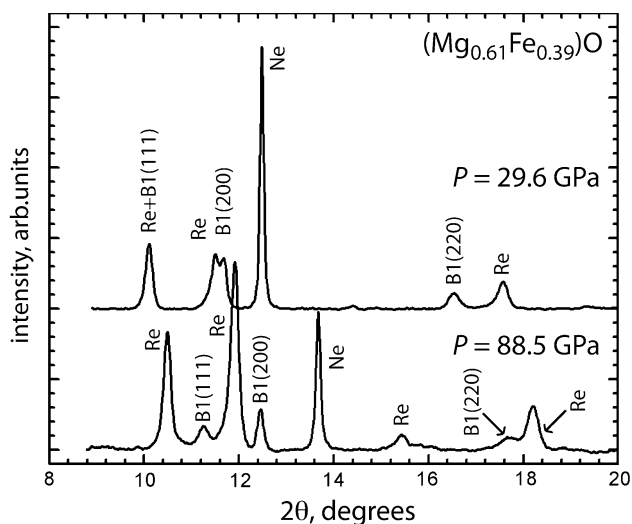


Fig. 8 Typical integrated X-ray spectra at different pressures for $(\text{Mg}_{0.61}\text{Fe}_{0.39})\text{O}$. At 29.6 GPa, we observe the 200 and 220 reflections from the B1 structure, and the 111 reflection is masked by a Re peak. At 88.5 GPa, the 220 reflection is significantly broadened

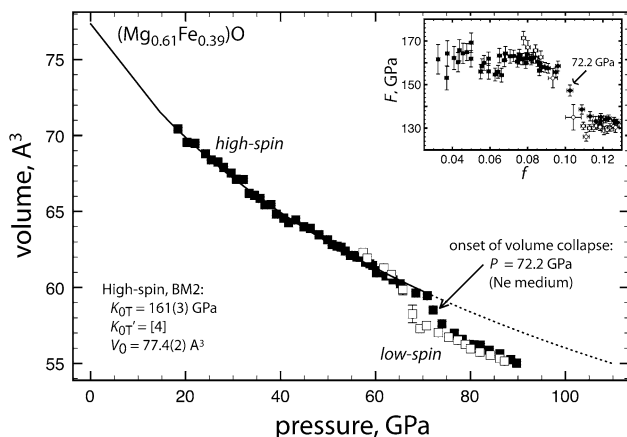


Fig. 9 P - V data for $(\text{Mg}_{0.61}\text{Fe}_{0.39})\text{O}$ using neon as a pressure medium (Table 5). The solid line is a second-order Birch-Murnaghan EOS fit to compression data up to 70.9 GPa. Inset normalized pressure (F) Eulerian finite strain (f) using $V_0 = 77.4 \pm 0.2 \text{ \AA}^3$. Note the trajectory change in the P - V data and F - f data around $P = 72.2 \text{ GPa}$ ($f = 0.102$ and $F = 147 \text{ GPa}$). Solid and open symbols refer to compression and decompression data, respectively

differs from those of previous studies in which similar compositions were investigated using NaCl and laser-annealing (Fei et al. 2007) or no medium (Speziale et al. 2005). In these studies, the onset of the spin crossover was observed at lower pressures. The offset is too large to be accounted for by using different pressure scales. Such a difference can be explained by the sensitivity of magnetic crossovers in $(\text{Mg,Fe})\text{O}$ to differential stress and perhaps thermal cycling (Kantor et al. 2009). Lin et al. (2005) reported the P - V behavior of $(\text{Mg}_{0.83}\text{Fe}_{0.17})\text{O}$ in a neon pressure medium to over 100 GPa and reported the onset of

Table 6 Equation of state parameters for high-spin $(\text{Mg}_{0.61}\text{Fe}_{0.39})\text{O}$ using different types of EOS in the pressure range up to 70.9 GPa

	V_0 (\AA^3)	K_{0T} (GPa)	K_{0T}'	χ_w^2
Cubic phase (B1, $Fm\bar{3}m$): high-spin state				
B-M 2d order	77.4(2)	161(3)	[4]	2.5
Vinet	77.2(2)	166(3)	[4]	2.5
B-M 3d order	77.7(9)	153(25)	4.2(7)	2.6
Vinet	77.8(9)	147(27)	4.6(9)	2.6

Numbers in parentheses indicate the esd's for the last digit for the last reported significant digit(s). Numbers in square brackets are fixed in the fitting procedure

the crossover to be at 55 GPa. Restricting the evaluation of the effect of iron on the paramagnetic (high-spin) to diamagnetic (low-spin) crossover to studies using neon as a pressure medium, we find higher crossover pressures for pyrolite-like $(\text{Mg,Fe})\text{O}$ compositions at 300 K, compared to studies using NaCl or no pressure medium. Upon decompression, the transition back to the high-spin state (based on P - V trajectory) was completed at about 65 GPa. We therefore bracket the spin crossover at $65 \leq P$ (GPa) ≤ 77 at 300 K (Fig. 9). There was no hysteresis reported in the study using NaCl and laser-annealing (Fei et al. 2007). However, the stress state in the different sample chambers cannot be determined accurately. It is clear that the obvious difference between the two studies is the thermal history of the sample, and recent studies have shown that the spin crossover pressure is highly dependent on thermal cycling (Kantor et al. 2009). Although neon as a pressure medium is soft relative to alternative media like NaCl or argon, neon is a solid at these pressures. The hysteresis observed in our study is likely due to the build up of strain in the crystallites. The resulting hysteresis can be viewed as a low-spin metastable state persisting until the Jahn-Teller distortion of the high-spin state is favored within the stress state of the sample's environment.

Acknowledgments We thank E. Hamecher (Caltech) for help with conducting experiments, S. Mackwell (Lunar & Planetary Institute, TX) for synthesizing and providing the $(\text{Mg}_{0.22}\text{Fe}_{0.78})\text{O}$ sample. The powdered $(\text{Mg}_{0.61}\text{Fe}_{0.39})\text{O}$ sample was synthesized with the help of Y. Fei (Carnegie Institution of Washington). I. Kantor and an anonymous reviewer provided helpful suggestions that improved the manuscript. This work was supported by the National Science Foundation EAR Geophysics 0711542 (JMJ). The Advanced Light Source is supported by the Director, Office of Science, Office of Basic Energy Sciences, of the U.S. Department of Energy under Contract No. DE-AC02-05CH11231. Portions of this work were supported by COMPRES under NSF Cooperative Agreement EAR 06-49658.

References

Angel RJ (2000) Equations of state. In: Hazen RM, Downs RT (eds) High-pressure and high-temperature crystal chemistry. (Reviews

- in Mineralogy and Geochemistry) Mineralogical Soc America, Washington, DC, pp 35–60
- Auzende AL, Badro J, Ryerson FJ, Weber PK, Fallon SJ, Addad A, Siebert J, Fiquet G (2008) Element partitioning between magnesium silicate perovskite and ferropericlase: new insights into bulk lower-mantle geochemistry. *Earth Planet Sci Lett* 269:164–174
- Badro J, Fiquet G, Guyot F, Rueff JP, Struzhkin VV, Vanko G, Monaco G (2003) Iron partitioning in Earth's lower mantle: toward a deep lower mantle discontinuity. *Science* 300:789–791
- Bower D, Gurnis M, Jackson JM, Sturhahn W (2009) Enhanced convection and fast plumes in the lower mantle induced by the spin transition in ferropericlase. *Geophys Res Lett*. doi: [10.1029/2009GL037706](https://doi.org/10.1029/2009GL037706)
- Crowhurst JC, Brown JM, Goncharov AF, Jacobsen SD (2008) Elasticity of (Mg, Fe)O through the spin transition of iron in the lower mantle. *Science* 319(5862):451–453
- Duffy TS, Hemley RJ, Mao HK (1995) Equation of state at multimegabar pressures: magnesium oxide to 227 GPa. *Phys Rev Lett* 74:1371–1374
- Fei Y, Zhang L, Corgne A, Watson HC, Ricolleau A, Meng Y, Prakapenka V (2007) Spin transition and equations of state of (Mg, Fe)O solid solutions. *Geophys Res Lett* 34:L17307
- Hammersley AP, Svenson SO, Hanfland M (1996) Two-dimensional detector software: from real detector to idealised image or two-theta scan. *High Pressure Res* 14:235–248
- Irfune T (1994) Absence of an aluminous phase in the upper part of the Earth's lower mantle. *Nature* 370:131–133
- Jacobsen SD, Reichmann HJ, Spetzler HA, Mackwell SJ, Smyth JR, Angel RJ, McCammon CA (2002) Structure and elasticity of single-crystal (Mg, Fe)O and a new method of generating shear waves for gigahertz ultrasonic interferometry. *J Geophys Res Solid Earth* 107:B2
- Jacobsen SD, Spetzler H, Reichmann HJ, Smyth JR (2004) Shear waves in the diamond-anvil cell reveal pressure-induced instability in (Mg, Fe)O. *Proc Natl Acad Sci USA* 101(16):5867–5871
- Jacobsen SD, Lin JF, Angel RJ, Shen G, Prakapenka V, Dera P, Mao HK, Hemley RJ (2005) Single-crystal synchrotron X-ray diffraction study of wüstite and magnesiowüstite at lower-mantle pressures. *J Synchrotron Radiat* 12:577–583
- Jacobsen SD, Holl CM, Adams KA, Fischer RA, Martin ES, Bina CR, Lin JF, Prakapenka VB, Kubo A, Dera P (2008) Compression of single-crystal magnesium oxide to 118 GPa and a ruby pressure gauge for helium pressure media. *Am Miner* 93:1823–1828
- Jeanloz R, Ahrens TJ (1980) Equations of state of FeO and CaO. *J R Astron Soc* 62:505–528
- Kantor AP, Jacobsen SD, Kantor IY, Dubrovinsky L, McCammon CA, Reichmann HJ, Goncharenko IN (2004) Pressure-induced magnetization in FeO: evidence from elasticity and Mössbauer spectroscopy. *Phys Rev Lett* 93:93215502
- Kantor I, Dubrovinsky L, McCammon C, Steinle-Neumann G, Kantor A, Skorodumova N, Pascarelli S, Aquilanti G (2009) Short-range order and Fe clustering in Mg_{1-x}Fe_xO under high pressure. *Phys Rev B* 80:014204
- Knittle E, Jeanloz R (1986) High-pressure metallization of FeO and implications for the Earth's core. *Geophys Res Lett* 96:16169–16180
- Kondo T, Ohtani E, Hirao N, Yagi T, Kikegawa T (2004) Phase transitions of (Mg, Fe)O at megabar pressures. *Phys Earth Planet Interiors* 143–144:201–213
- Larsen AC, Von Dreele R (2000) General structure analysis system (GSAS), Los Alamos National Laboratory, Los Alamos
- Lin JF, Heinz DL, Mao HK, Hemley RJ, Devine JM, Li J, Shen GY (2003) Stability of magnesiowüstite in Earth's lower mantle. *Proc Natl Acad Sci USA* 100(8):4405–4408
- Lin JF, Struzhkin VV, Jacobsen SD, Hu M, Chow P, Kung J, Liu H, Mao HK, Hemley RJ (2005) Spin transition of iron in magnesiowüstite in the Earth's lower mantle. *Nature* 436:377–380
- Lin JF, Jacobsen SD, Sturhahn W, Jackson JM, Zhao J, Yoo CS (2006) Sound velocities of ferropericlase in the Earth's lower mantle. *Geophys Res Lett* 33. doi: [10.1029/2006GL028099](https://doi.org/10.1029/2006GL028099)
- Mackwell SJ, Bystricky M, Sproni C (2005) Fe–Mg interdiffusion in (Mg, Fe)O. *Phys Chem Miner* 32:418–425
- Mao HK, Xu J, Bell PM (1986) Calibration of the ruby pressure gauge to 800 kbar under quasi-hydrostatic conditions. *J Geophys Res* B91:4673–4676
- Mao HK, Shu J, Fei Y, Hu J, Hemley RJ (1996) The wüstite enigma. *Phys Earth Planet Interiors* 96:135–145
- Mao WL, Shu J, Hu J, Hemley RJ, Mao HK (2002) Displacive transition in magnesiowüstite. *J Phys Condens Matter* 14:11349–11354
- Marquardt H, Speziale S, Reichmann HJ, Frost DJ, Schilling FR, Garnero EJ (2009) Elastic shear anisotropy of ferropericlase in Earth's lower mantle. *Science* 324(5924):224–225. doi: [10.1126/science.1169365](https://doi.org/10.1126/science.1169365)
- McDonough WF, Sun SS (1995) The composition of the Earth. *Chem Geol* 120:223–253
- Murakami M, Hirose K, Sata N, Ohishi Y (2005) Post-perovskite phase transition and mineral chemistry in the pyrolytic lowermost mantle. *Geophys Res Lett* 32. doi: [10.1029/2004GL021956](https://doi.org/10.1029/2004GL021956)
- Persson K, Bengtson A, Ceder G, Morgan D (2006) Ab initio study of the composition dependence of the pressure-induced spin transition in the (Mg_{1-x}Fe_x)O system. *Geophys Res Lett* 33(16):L16306
- Richet P, Mao HK, Bell PM (1989) Bulk moduli of magnesiowüstite from static compression experiments. *J Geophys Res* 94:3037–3045
- Rivers M, Prakapenka VB, Kubo A, Pullins C, Holl CM, Jacobsen SD (2008) The COMPRES/GSECARS gas-loading system for diamond anvil cells at the Advanced Photon Source. *High Press Res* 28(3):273–292
- Shu J, Mao HK, Hu J, Fei Y, Hemley RJ (1998) Single-crystal X-ray diffraction of wüstite to 30 GPa under hydrostatic pressure. *Neues Jahrb Miner Abh* 172(2–3):309–323
- Sinmyo R, Hirose K, Nishio-Hamane D, Seto Y, Fujino K, Sata N, Ohishi Y (2008) Partitioning of iron between perovskite/postperovskite and ferropericlase in the lower mantle. *J Geophys Res* 113:B11204. doi: [10.1029/2008JB005730](https://doi.org/10.1029/2008JB005730)
- Speziale S, Milner A, Lee VE, Clark SM, Pasternak MP, Jeanloz R (2005) Iron spin transition in Earth's mantle. *Proc Natl Acad Sci USA* 102(50):17918–17922
- Speziale S, Lee VE, Clark SM et al (2007) Effects of Fe spin transition on the elasticity of (Mg, Fe) O magnesiowüstites and implications for the seismological properties of the Earth's lower mantle *J Geophys Res* 112(B10):B10212
- Struzhkin VV, Mao HK, Hu JZ, Schwoerer-Bohning M, Shu JF, Hemley RJ, Sturhahn W, Hu MY, Alp EE, Eng P, Shen GY (2001) Nuclear inelastic X-ray scattering of FeO to 48 GPa. *Phys Rev Lett* 87:25. doi: [10.1103/PhysRevLett.87.255501](https://doi.org/10.1103/PhysRevLett.87.255501)
- Sturhahn W, Jackson JM, Lin JF (2005) The spin state of iron in minerals of Earth's lower mantle. *Geophys Res Lett* 32:L12307. doi: [10.1029/2005GL022802](https://doi.org/10.1029/2005GL022802)
- Toby BH (2001) EXPGUI, a graphical user interface for GSAS. *J Appl Crystallogr* 34:210–213
- Tschiya T, Wentzcovitch RM, CRSd Silver, Gironcoli SD (2006) Spin transition is magnesiowüstite in Earth's lower mantle. *Phys Rev Lett* 96:198501
- Zha CS, Mao HK, Hemley RJ (2000) Elasticity of MgO and a primary pressure scale to 55 GPa. *Proc Natl Acad Sci USA* 97(25):13494–13499